RSC Advances

ROYAL SOCIETY OF CHEMISTRY

www.rsc.org/advances

Journal Name

ARTICLE

Preparation of chestnut-like porous NiO nanosphere as electrodes for supercapacitors

Received 00th January 20xx,
Accepted 00th January 20xx

DOI: 10.1039/x0xx00000x

www.rsc.org/

Feng Yu [a,b], Li Zhu [a], Ting You [a], Faxing Wang [b], Zubiao Wen [a,]†,

Chestnut-like porous nanosphere (CPN) NiO was preparation by a simple hydrothermal method. The electrochemical tests indicate that the NiO electrodes exhibit a reversible capacitance of 982 F g^{-1} at current density of 1A g^{-1} in 6 M KOH electrolyte. When assembling supercapacitor with activate carbon (AC), the supercapacitor of AC/6M KOH/NiO can deliver an energy density of 51.5 Wh kg^{-1} at 0.38 kW kg^{-1} and even maintain 27.7 Wh kg^{-1} at 2.32 kW kg^{-1}. In addition, it cycling behavior can achieve 10000 times in 6M KOH electrolyte. This excellent performance demonstrate that the chestnut-like porous NiO nanosphere will be of great promise for supercapacitors applied to large power devices such as electric vehicle.

1. Introduction

In the past decades, supercapacitors have attracted much attention because of a lot of excellent characteristics, such as the broader working temperature, long lifecycle, shorter charging time, high power density and low cost.[1-4] Supercapacitors also call electrochemical capacitors, it is the bridge in tradition capacitors and battery.[5-8] According to the different charge-storage mechanisms, supercapacitors can be divided into electric double layer capacitor (EDLC) and pseudo-capacitors.[9-11] In this two kinds capacitors, the former is mainly using carbon-based materials as electrodes, such as high specific areas activated carbon,[12] graphene,[13] CNTs,[14] the other is mainly using metal oxides/hydroxides (such as NiO/$Ni(OH)_2$, MnO_2, Co_3O_4/$Co(OH)_2$, RuO_2, V_2O_5),[15-20] metal sulfides,[21,22] conduction polymers[23-25] and their composites.[26-30] Among the explored materials, NiO has been widely thought a promising electrode materials because it is less expensive, easy availability and have high theoretical value of 2573 F g^{-1}.[31]

In this work, we prepared the chestnut-like porous NiO by a simple hydrothermal method. The electrochemical tested results show that the chestnut-like porous NiO as electrode material have excellent electrochemical performance. The specific capacitance can be achieved to 982 F g^{-1} at current density of 1 A g^{-1}. Moreover, its capacitance retention is 92.6% after 10000 cycles at tested current density of 1 A g^{-1}

2. Experimental

2.1 Preparation of materials

Chestnut-like porous nanosphere (CPN) NiO was synthesized by a simple hydrothermal method. Briefly, 2 mmol $Ni(NO_3)_2 \cdot 6H_2O$ and 20 mmol urea were dissolved in 40 mL deionized water with stirred for 20 min. Then, the reaction solution was transferred into a 50 mL Teflon-lined stainless steel autoclave and kept in a drying oven at 110 °C for 3 h. Finally, the obtained precipitate was collected by suction filtration, washed 2-3 times with ultrapure ethanol and deionized water, and dried at 80°C under vacuum for 12 h. The growth process for NiO consists of two steps: (1) hydrolysis reaction of the urea upon heating at 110 °C to form aqueous ammonia (NH_4OH) solution, which can be expressed through the following reaction:

$$CO(NH_2)_2 + H_2O \rightarrow CO_2 + NH_4OH \quad (1)$$

and (2) precipitation of $Ni(OH)_2$ via the reaction of $Ni(NO)_3$ with NH_4OH solution through the following proposed reaction:

$$Ni(NO_3)_2 + 2NH_4OH \rightarrow Ni(OH)_2 \downarrow + 2NH_4^+ + 2NO_3^- \quad (2)$$

2.2 Characterization of the as-prepared materials

Morphological analyses of samples were carried out on a Philip XL30 scanning electron micrographs (SEM) and a JEOL JEM-2010 transmission electron microscope (TEM). XRD patterns were collected using a Rigaku D/MAX-IIA X-ray diffractometer with Cu Kα radiation. The specific surface area of the samples was calculated using nitrogen adsorption/desorption isotherms which were obtained at 77K on a Nova 1000. X-ray photoelectron spectroscopy (XPS) analysis of the sample was carried out on a VG ESCALAB MK2 spectroscope used Al Kα X-rays as the excitation source with a voltage of 12.5 kV and power of 250 W. The working electrode was prepared by pressing a mushy mixture of the as-prepared NiO or activated carbon, acetylene black and poly(tetrafluoroethylene) (PTFE) (in a weight ratio of 8:1:1) dispersed in ethanol onto Ni-grid. The cyclic voltammetry (CV) and galvanostatic charge-discharge (GCD) tests of the electrode were performed using a three-electrode cell, where Ni-grid and saturated calomel electrode were used as the counter and reference electrodes, respectively. The electrochemical impedance spectra (EIS) were recorded from 10^5 to 10^{-2} Hz and the amplitude of the used perturbation was 5 mV. The two-electrode asymmetric supercapacitors of AC//NiO was also assembled and measured in 6 M KOH aqueous electrolyte. All the

[a] College of Chemistry and Chemical Engineering, Jiangxi Normal University, Nanchang 330022, China
[b] College of Energy, Nanjing Tech University, Nanjing 211816, Jiangsu Province, China
† Correspondence authors: wenzubiao@163.com (Wen),
See DOI: 10.1039/x0xx00000x

electrochemical measurements were performed at ambient temperature. Electrochemical performance was tested without the removal of the oxygen from the solution.

3. Results and discussion

The Fig.1a-c are the morphologies of NiO. The insert picture at the Fig. 1a is chestnut fruit like the sample in this paper. It can be clearly seen that chestnut NiO are nanosphere and the average size of this sample is about 800 nm (Fig. 1b). TEM micrographs (Fig. 1c) further confirm the configuration of the core-shell structure of NiO. It has much of nanosheets that are formed with about 100 nm in size and about 20 nm in thickness at the surface of the core-shell structured. This unique and ordered core-shell structured provides an abundant porous surface area for the contact between the electrode and electrolyte, which is of great significance in accelerating the electrochemical reactions. The crystal phase of the NiO was analyzed by powder X-ray diffraction (XRD). The XRD pattern of CPN-NiO is shown in Fig. 1d. The four identified diffraction peaks at 37.2°, 43.2°, 62.7° and 75.3° corresponding to the (111), (200), (220) and (311) planes of cubic phase of NiO.[32]

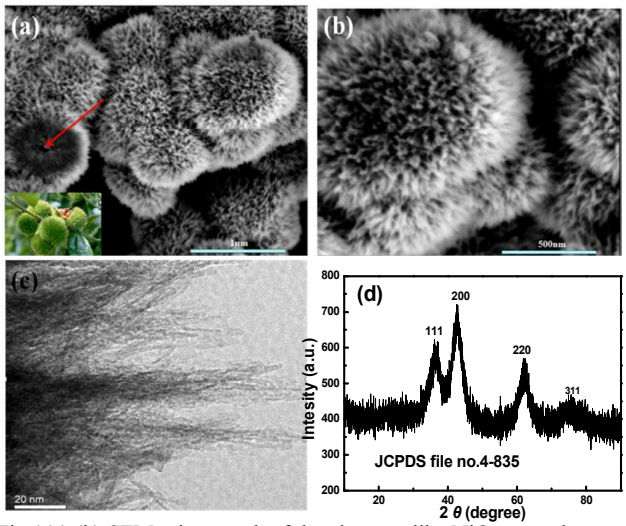

Fig.1(a) (b) SEM micrograph of the chestnut-like NiO nanosphere at different dimension, (c) TEM micrograph of the virginal NiO nanosphere at different dimension. (d) XRD pattern of the NiO nanocomposite

The porosity and surface area of the CPN-NiO was investigated through N_2 adsorption-desorption isotherm studies (Fig. 2a), which exhibit Brunauer-Deming-Deming-Teller (BDDT) type IV shape of isotherms with a H3-type hysteresis loop according to the IUPAC classification. The fitting based on the Brunauer-Emmett-Teller (BET) equation reveals the surface area of the CPN-NiO is 174.1 m^2 g^{-1}. Such big specific surface area may greatly improve the accessibility of material to electrolyte ions and diffusion of electrons by providing an efficient transport pathway and more adsorption sites in the interior of the electrode, which is helpful to enhance specific capacitance of CPN-NiO electrode.

The chemical composition and the valence state of the element in the CPN-NiO were further investigated by X-ray photoelectron spectroscopy. The Ni 2p region (Fig. 2b) comprises four easily discernible features: the Ni $2p_{3/2}$ main peak and its satellite at 854.1 and 861.5 eV, and the Ni $2p_{1/2}$ main peak and its satellite at 871.9 and 879.2 eV, respective, which are agreement with reported data of NiO[33] and confirm that Ni is in the +2 oxidation state.

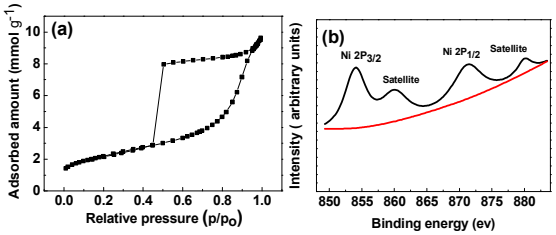

Fig. 2.(a) N_2 adsorption-desorption isotherms of the CPN-NiO. (b) XPS spectra of the Ni 2p region for CPN-NiO

The CV measurements were conducted in a 6 M KOH solution as the electrolyte and the scanning rates at 5, 10, 20, 30 mV s^{-1} in potential range of 0-0.5 V are plotted in Fig. 3a. The results show the CV curves have anodic and cathodic peaks, which are character of the pseudocapacitors. The anodic peak in CV curved shifted toward positive potential with increase in the scanning rate, on the other hand the cathodic peak shift toward negative potential on account of the polarization in the electrode material. The redox mechanism can be explained to NiO/NiOOH redox pair.[34]

$$NiO + OH^- \Leftrightarrow NiOOH + e^- \qquad (3)$$

The inset in Fig. 3a is variation of anodic peak current (i) with the square root of scan rate (v), which agrees with $i \propto v^{-1/2}$. Therefore, the capacitance was predominated by the bulk diffusion process.[35] The galvanostatic charge/discharge tests of the electrode were conducted at current densities from 1 to 10 A g^{-1} in the potential range of 0-0.4 V. The current-time curves (Fig. 3b) show that CPN-NiO have an evident charge and discharge platforms located at about 0.28 V and 0.15 V, respectively. According the discharge specific capacity C (F g^{-1}) is calculated equation (4):

$$C = (I \Delta t) / (m \Delta V) \qquad (4)$$

Where I (mA) is the applied working current, Δt (s) represents the discharge time, ΔV (V) is the voltage range, and m (mg) is the mass of active materials

The specific capacitance is calculated to be 982, 817, 713, 641, 571, 509, 445, 385, 320 and 276 F g^{-1} corresponding to the discharge current densities 1, 2, 3, 4, 5, 6, 7, 8, 9 and 10 A g^{-1} (Fig. 3c), the specific capacitance of chestnut-like porous NiO can up to 982 F g^{-1} at 1A g^{-1}, it can clearly be seen that the values are larger than most of those of earlier report[Table 1].[35-48] It can be ascribe to that unique and ordered core-shell structured and larger specific surface area, which can be provides an abundant porous surface area for the contact between the electrode and electrolyte, and accelerating the electrochemical reactions. In addition, the coulombic efficiency more than 100% at current density 1A g^{-1} is appreciable, which can be explained by eq 3. In discharging process only a part of NiOOH gains electron and get reduced into NiO, while in charging process NiO loses electron and completely oxidized into NiOOH. Since, NiOOH is partially convert into NiO during reduction, the unconverted NiOOH holds the electrons during discharging and thus the discharging takes longer time.[48] To confirm the electrochemical stability of the electrode, the charge/discharge has be tested 10000 times at current density 1A g^{-1}, Fig. 3d presents that the electrode have good cycling behaviour with a litter lost of capacitance at the end of 10000 cycles (92.6% of capacitance retention). The

coulombic efficiency is near to 100%. All the above tests indicate that the NiO nanosheet can be used as an excellent electrode material for supercapacitors.

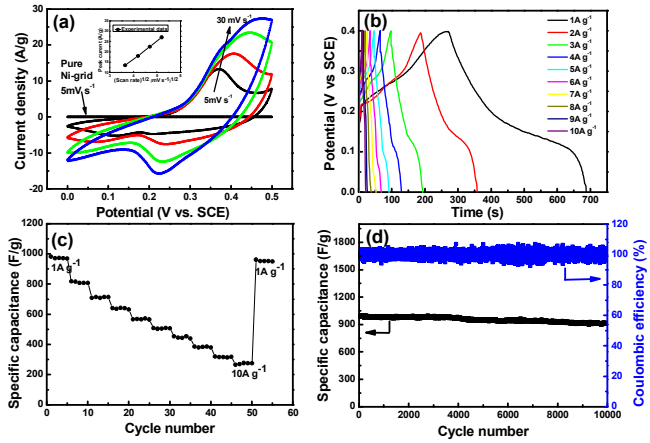

Fig. 3(a), Cyclic voltammograms of NiO at the different scan rate and pure Ni-grid at scan rate 5 mV s^{-1}, (b) glvanostatic charge-discharge curves of the NiO at different current densities, (c) variation of specific capacitance with discharge current density for NiO and (d) The cycling behavior of NiO at 1A g^{-1}. All tested are in the 6 M KOH electrolyte.

Materitals	Method	Specific capacitance	Capacitive retention(%)	References
Nanosphere NiO	Hydrothermal	982 F g^{-1}	92.6/10000	This work
Hierarchical porous NiO nanotube	Electrodeposition	675 F g^{-1}	93.2/10000	35
Electrospun NiO nanowires	Electrospinning	670 F g^{-1}	89/3000	34
Porous NiO nanosheets	Multistep preparation	600 F g^{-1}	--/1000	36
Porous NiO/VN	Solid reaction	680 F g^{-1}	85/1000	37
Mesoporous NiO nanoflake	Reflux precipitation	428 F g^{-1}	--/5000	38
G/NiO	Hydrothermal	530 F g^{-1}	92/5000	39
NiO	Urea-controlled hydrothermal method	609 F g^{-1}	62/5000	40
Mesoporous NiO nanosheets	Self-assembled	1060 F g^{-1}	91/5000	41
NiO	Hydrothermal	250 F g^{-1}	75/2000	42
Flowerlike NiO	Hydrothermal	923 F g^{-1}	89/1000	43
NiO nanoparticle	Solgel method	549 F/g	81.8/1000	44
NiO nanopetal	Anodization	378 F g^{-1}	92.2/10000	45
H-Ni/NiO core-shell	Hydrogenated	1635 F g^{-1}	57/1200	46
H-NiO nanoblock	Hydrogenated	1272 F g^{-1}	94.7/3000	47

Table 1. Comparative representation of different aspects of NiO for supercapacitor.

The electrochemical impedance spectroscopy (EIS) analyses were carried out to examine charge transfer rate of electrolyte ions for the CPN-NiO electrode. The Nyquist plot of the CPN-NiO electrode in the frequency range from 10^5 to 10^{-2} Hz is shown in the Fig 4. The impedance spectra have a straight line and semicircular arc. The measured impedance spectra were analyzed using the complex nonlinear least squares fitting method on the basis of the equivalent circuit, which is given in the inset of Fig. 4. The X-intercept of the Nyquist plots corresponds to the equivalent series resistance (R_s), which contains the contributions of ionic and electronic resistance.[48]

The intrinsic resistance of the material is in connection with electronic resistance, while the interfacial resistance is an integration of the resistance among current collector and particles and resistance among the interparticles. The incorporation of a constant phase element (CPE) in the equivalent circuit corresponds to the porosity of the electrode and the semi-infinite diffusion of the cations.[50] The diffusion resistance (ionic resistance) of the electrolyte resistance in the pores and ionic through pores are coupled with diffusion resistance. The high-frequency region presenting a semicircle arc is a result of the charge transfer resistance (R_{ct}), which can be divided into the double layer capacitance (C_{dl}) at the electrode/electrolyte interface and the faradaic reactions. From the diameter of the semicircular arc the R_{ct} can be calculated. The measured value of the R_s and R_{ct} for the CPN-NiO electrode is 1.75 and 8.90 Ω cm^{-2}, respectively. The smaller values of R_s and R_{ct} are due to the porous nanostructure of electrode facilitating the effective access of electrolyte ions in the active electrode material and shortening the ion diffusion path.

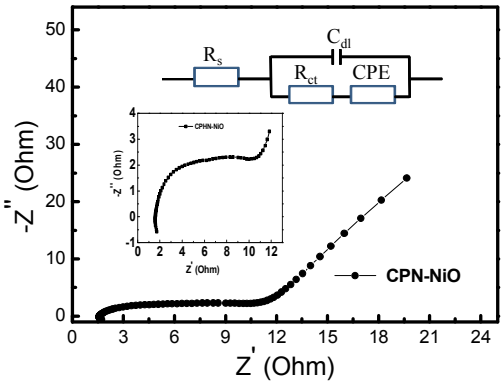

Fig. 4 Nyquist plots of the CPN-NiO in 6 M KOH aqueous solution with the amplitude of 5 mV in the frequency range from 10^5 to 10^{-2} Hz by using a Ni-grid as the counter electrode and a saturated calomel electrode (SCE) as the reference electrode.

According to the following equation (5):

$$1/C=1/C_1+1/C_2 \qquad (5)$$

Where C is the capacitance of supercapacitor, C_1 and C_2 are capacitance of positive and negative electrodes, respectively. When the weight ratios of CPN-NiO to the AC is 1 : 3, the hybrid supercapacitor system can obtain the largest capacitance. When the electrode materials of the CPN-NiO was built up a supercapacitor with AC (activated carbon) as the negative electrode, the galvanostatic charge/discharge behaviors of the AC/6 M KOH/CPN-NiO composite at current density at 1 A g^{-1} is shown in Fig. 5a. The charge/discharge voltage range for the supercapacitors is from 0 to 1.5 V. The charge and discharge curves are basically symmetric, which implies that the ideal capacitive behaviors for the supercapacitor. The Ragone plots of the AC/6 M KOH/CPN-NiO asymmetric supercapacitor is shown in Fig. 5b. All the date was calculated on the basis of the total mass. The energy and power densities were derived from galvanostatic charging and discharging at various current densities. The specific energy density (E) and power density (P) stored in such a capacitor are given by equations (6) and (7) [9]:

$$E = \int iVdt \qquad (6)$$

$$P = iV \qquad (7)$$

Where i was the constant current, V is the voltage at time t. As seen from the Ragone plots, the energy density of the asymmetric supercapacitor is 51.5 Wh kg^{-1} at 0.38 kW kg^{-1} on the basis of the total weight of NiO and AC, and even maintains at 27.7 Wh kg^{-1} at 2.32 kW kg^{-1} (Fig. 5b). To our most knowledge, such a high energy density is rarely reported for the supercapacitors based on alkali solutions.

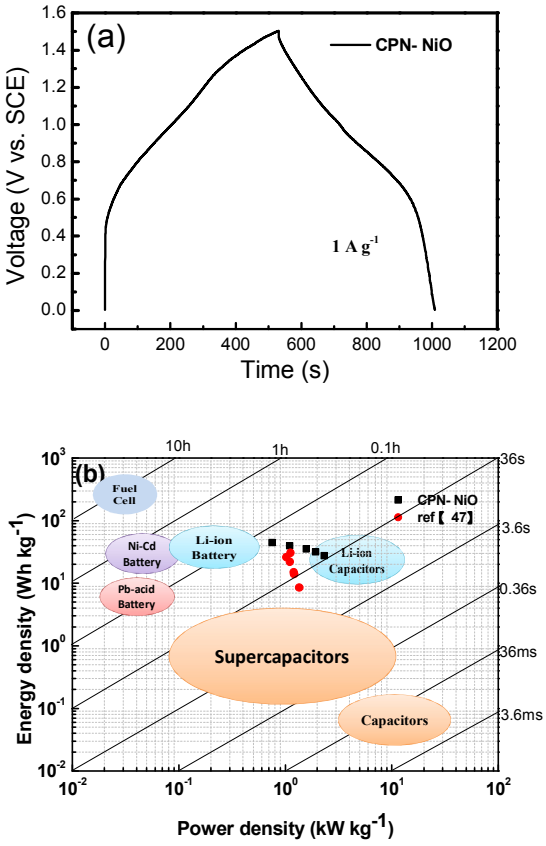

Fig. 5 (a) Potential-time curve of the AC//NiO supercapacitor at current density of 1 A g^{-1} in 6 M KOH aqueous electrolyte, and (b) Ragone plot of the AC//NiO supercapacitor.

Conclusions

In summary, Chestnut-like porous nanosphere NiO material was prepared by a simple hydrothermal method. The Chestnut-like porous nanosphere NiO is aggregate together from nanosheets with thickness of about 20 nm. The electrochemical tests show that the Chestnut-like porous nanosphere NiO has good performance in 6 M KOH electrolyte. The specific capacitance can be up to 982 F g^{-1} at current density of 1 A g^{-1} and with 92.6% of capacitance retention after 10000 cycles, which is good then other reports. When assemble supercapacitor with activate carbon (AC), the energy density of 51.5 Wh kg^{-1} at 383 W kg^{-1}. The results demonstrate that the Chestnut-like porous nanosphere NiO is promise electrode material for supercapacitor.

Acknowledgements

Financial supports from Science & Technology Support Program of Jiangxi Province (20142BAB203013) are gratefully appreciated.

Notes and references

1 P. Simon and Y. Gogotis, *Nat. Mater.*, 2008, **7**, 845-854.
2 G. Wang, L. Zhang and J. Zhang, *Chem. Soc. Rev.*, 2012, **41**, 797-828.
3 H. Jiang, P. S. Lee and C. Li, *Energy Environ. Sci.*, 2013, **6**, 41-53.
4 L. Peng, X. Peng, B. Liu, C. Wu, Y. Xie and G. Yu, *Nano Lett.*, 2013, **13**, 2151-2157.
5 R. Kotz and M. Carlen, *Electrochim. Acta*, 2000, **45**, 2483-2497.
6 A. S. Arico, P. Bruce, B. Scrosati, J. M. Tarascon and W. Schalkwijk, *Nat. Mater.*, 2005, **4**, 366-377.
7 B. E. Conway, *J. Electrochem. Soc.*,1991, **138**, 1539-1548.
8 M. Zhi, C. Xiang, J. Li, M. Li and N. Wu, *Nanoscale,* 2013, **5**, 72-88.
9 F. X. Wang, S. Y. Xiao, Y. Y. Hou, C. L. Hu, L. L. Liu and Y. P. Wu, *RSC Adv.*, 2013, **3**, 13059-13084.
10 Y. Zhai, Y. Dou, D. Zhao, P. F. Fulvio, R. T. Mayes and S. Dai, *Adv. mater.*, 2011, **23**, 4828-4850.
11 P. Simon and Y. Gogotis, *Acc. Chem. Res.*, 2013, **46**, 1094-1103.
12 S. L. Candelaria, Y. Shao, W. Zhou, X. Li, J. Xiao, J. G. Zhang, Y. Wang, J. Liu, J. H. Li and G. Z. Cao, *Nano Energy*, 2012, **1**, 195-220.
13 Y. Wang，Z. Q. Shi，Y. Huang, Y. F. Ma, C. Y. Wang, M. M. Chen and Y. S. Chen, *J. Phys. Chem. C*, 2009, **113**, 13103-13107.
14 C. M. Yang，Y. J. Kin，M. End，H. Kanoh，M. Yudasaka, S. Lijima and K. Kaneko, *J. Am. Chem. Soc.*, 2007, **129**, 20-21.
15 X. J. Liu, J. C. Zhao, Y. J. Cao, W. Y. Li, Y. Q. Sun, J. Lu, Y. Men and J. Q. Hu, *RSC Adv.*, 2015, **5**, 47506-47510.
16 J. Y. Cao, X. H. Li, Y. M. Wang, F. C. Walsh, J. H. Ouyang, D. C. Jia and Y. Zhuo, *J. Power Sources*, 2015, **293**, 657-74.
17 C. Xu, F. Kang, B. Li and H. Du, J. *Mater. Res*, 2011, **25**, 1421-1432.
18 X. C. Dong, H. Xu, X. W. Wang, Y. X. Huang, M. B. Chen, H. Zhang, L. H. Wang, W. Huang and P. Chen, *ACS Nano*, 2012, **6**, 3206-3213.
19 V. Subramanian, *Solid State Ionics*, 2004, **175**, 511-515.
20 B. Saravanakumar, K. K. Purushothaman and G. Muralidharan, *ACS Appl. Mater. Interfaces*, 2012, **4**, 4484-4490.
21 L. Ma, X. Shen, Z. Ji, S. Wang, H. Zhou and G. Zhu, *Electrochim. Acta*, 2014, **146**, 525-532.
22 J. Wang, D. L. Chao, J. L. Liu, L. L. Li, L. F. Lai, J. Y. Lin and Z. X. Shen, *Nano Energy*, 2014, **7**, 151-160.
23 D. Nandi, S. Nandi, P. K. Pal, A. K. Ghosh, A. De and U. C. Ghosh, *Appl. Surf. Sci.*, 2014, **293**, 90-96.
24 H. Gao and K. Lian, *RSC Adv.*, 2014, **4**, 33091-33113.
25 G. A. Snook, P. Kao and A. S. Best, *J. Power Sources*, 2011, **196**, 1-12.
26 U. Male and P. Srinivasan. *J. Appl. Poly. Sci*, DOI: 10.1002/app.42540.
27 S. D. Min, C. Q. Zhao, Z. M. Zhang, K. Wang, G. R. Chen, X. Z. Qian and Z. P. Guo, *RSC Adv.*, 2015, **5**, 62571-62576.
28 L. Zhu, W. Y. Wu, Y. S. Zhu, W. P. Tang and Y. P. Wu, *J. Phys. Chem. C*, 2015, **119**, 7069-7075.
29 X. Jiang, Y. C. Cao, P. X. Li, J. Q. Wei, K. L. Wang, D. H. Wu and H. W. Zhu, *Mater. Lett.*, 2015, **140**, 43-47.
30 W. Q. Ma, Q. Q. Shi, H. H. Nan, Q. Q. Hu, X. T. Zheng, B. Y. Geng and X. J. Zhang, *RSC Adv.*, 2015, **5**, 39864-39869.
31 C. Y. Chen, C. Q. Chen, P. P. Huang, F. F. Duan, S. C. Zhao, P. Li, J. C. Fan, W. G. Song and Y. Qin, *Nanotechnology*, 2014, **25**, 504001-504009.

32 J. Liang, H. Tan, C. Xiao, G. Zhou, S. Guo and S. Ding, *J. Power Sources*, 2015, **285**, 210-216.
33 M. A. Peck and M. A. Langell, *Chem. Mater.*, 2012, **24**, 4483-4490.
33 T. Meng, P. P. Ma, J. L. Chang, Z. H. Wang, T. Z. Ren, *Electrochim. Acta*, 2014, **125**, 586-592.
35 B. Vidhyadharan, N. K. M. Zain, I. I. Misnon, R. A. Aziz, J. Ismail, M. M. Yusoff and R. Jose, *J. Alloys Comp*, 2014, **610**, 143-150.
36 F. Cao, G. X. Pan, X. H. Xia, P. S. Tang and H. F. Chen, *J. Power Sources,* 2014, **264**, 161-167.
37 W. Yu, X. Jiang, S. Ding and B. Q. Li, *J. Power Sources*, 2014, **256**, 440-448.
38 Z. H. Gao, H. Zhang, G. P. Cao, M. F. Han and Y. S. Yang, *Electrochim. Acta*, 2013, **87**, 375-380.
39 X. Yan, X. Tong, J. Wang, C. Gong, M. Zhang and L. Liang, *J. Alloys Comp.*, 2014, **593**, 184-189.
40 P. Deng, H. Y. Zhang, Y. M. Chen, Z. H. Li, X. F. Xu, Y. Y. Li and Z. C. Shi, *J. Alloys Comp.*, 2015, **644**, 165-171.
41 G. Cheng, Y. N. Yan and R. Chen, *New J. Chem.*, DOI: 10.1039/c4nj01398k
42 M. M. Yao, Z. H. Hu, Z. J. Xu, Y. F. Liu, P. P. Liu and Q. Zhang , *J. Power Sources*, 2015, **273**, 914-922.
43 Y. Jiang, X. J. Leng, Z. L. Jia, H. X. Chen, H. Suo and C. Zhao, *J.Mater Sci: Mater Electron.,* 2015, **26**, 2995-3000.
44 Y. Y. Zhang, Y. Liu, Y. P. Guo, Y. X. Yeow, H. N. Duan, H. Li and H. Z. Liu, *Mater. Chem Phys.*, 2015, **151**, 160-166.
45 S. P. Jahromi, A. Pandikumar, B. T. Goh, Y. S. Lim, W. J. Basirun, H. N. Lim and N. M. Huang, *RSC Adv.*, 2015, **5**, 14010-14019.
46 G. H. Cheng, Q. G. Bai, C. H. Si, W. F. Yang, C. Q. Dong, H. Wang, Y. L. Gao and Z. H. Zhang, *RSC Adv.*, 2015, **5**, 15042-15051.
47 A. K. Singh, D. Sarkar, G. G. Khan and K. Mandal, *J. Mater Chem A.* 2013, **1**, 12759-12767.
48 A. K. Singh, D. Sarkar, G. G. Khan and K. Mandal, *ACS Appl. Mater. Interfaces*, 2014, **6**, 4684-4692.
49 G. S. Gund, D. P. Dubal, S. S. Shinde and C. D. Lokhande, *ACS Appl. Mater. Interfaces*, 2014, **6**, 3176-3188.
50 D. P. Dubal, G. S. Gund, C. D. Lokhande and R. Holze, *ACS Appl. Mater. Interfaces*, 2013, **5**, 2446-2454.